Multi-qubit entanglement generation with squeezed modes

Alexandru Macridin,¹ Andrew Cameron,¹ Cristian Pena,¹ Si Xie,¹ Raju Valivarthi,² and Panagiotis Spentzouris¹

¹ Fermi National Accelerator Laboratory, Batavia, IL, 60510, USA

² Division of Physics, Mathematics and Astronomy,

California Institute of Technology, Pasadena, California 91125, USA

We present a hybrid continuous variable-discrete variable entanglement generation protocol using linear optics and homodyne measurements, capable of producing multiple high-fidelity Bell pairs per protocol iteration, with an approximate 0.5 success probability. The effectiveness of the protocol is determined by the squeezing strength. To increase the number of Bell pairs, approximately 3 dB of extra squeezing is needed for each additional Bell pair. The protocol also generates single Bell pairs with an approximate 0.75 probability for squeezing strengths $\lesssim 15dB$, achievable with current technology.

I. Introduction

Emerging quantum technologies, such as quantum networks and the quantum internet, require entanglement distribution over long distances and at high rates. Most entanglement distribution methods rely fundamentally on entanglement generation protocols (EGPs) and entanglement swapping protocols (ESPs) [1–3]. In this paper, we introduce a hybrid continuous-variable (CV)–discrete-variable (DV) entanglement generation protocol that employs squeezed optical modes, linear optics, and homodyne measurements. In this protocol, local entanglement between squeezed light modes and multi-qubit nodes is swapped via homodyne measurement of the optical modes, resulting in the creation of multiple Bell pairs per iteration between spatially separated multi-qubit nodes. The protocol can be readily integrated into subsequent quantum repeater and networking schemes.

The most feasible way for current technology to implement an ESP is by using linear optical elements to transmit and measure information encoded in photonic degrees of freedom. The common example is the implementation of an ESP with photonic qubits [2], which requires a Bell state measurement (BSM). However, one major drawback of the ESP with photonic qubits and linear optics is that the BSM is non-deterministic, leading to a success probability that does not exceed 0.5 [4–6]. Additionally, quantum networks are plagued by signal loss across optical fibers, BSM errors, memory decoherence, classical communication delays, and other issues. All these factors further decrease the success probability and limit the Bell pair transmission rate.

A large research effort is currently underway to increase the entanglement generation rate. This is being pursued by developing new networking protocols using existing entanglement swapping and distillation protocols (for example, multiplexing and parallelization schemes), or by developing new EGP methods. There are many proposals in the literature to increase the success probability or to overcome the non-deterministic nature of an EGP with optical modes, including photon hyperentanglement [7], non-linear photonic interactions [8–12], optical squeezing [13], or the inclusion of ancillary photonic qubits [14, 15]. Hybrid DV-CV protocols, which leverage the interaction between qubits and a coherent optical mode combined with homodyne measurement [16], cat-state projection, and single-photon detection [17], have been proposed for the nondeterministic generation of a single Bell pair and subsequently used in quantum repeaters. Unlike these hybrid approaches, our hybrid DV-CV protocol utilizes squeezed light instead of coherent light and enables entanglement between multiple pairs of qubits per homodyne measurement and subsequent local operations.

We present a hybrid DV-CV nondeterministic protocol for generating multiple Bell pairs between two distant nodes. At two different locations, a multi-qubit node is entangled with a squeezed CV mode. The two CV modes are then transmitted to a third location, where they pass through a 50 : 50 beam splitter, and their quadratures are measured using homodyne detection. Local qubit operations, dependent on the measurement outcome, are then performed at each node. Unlike common photonic-qubit-based protocols, which generate one Bell pair per transmitted and measured signal, our protocol entangles multiple (n_b) Bell pairs per protocol iteration with a finite success probability. The effectiveness of the protocol is determined by the squeezing strength. The success probability decreases with decreasing squeezing. For a fixed success probability, the required squeezing, measured in decibels, scales linearly with n_b . We find that $10 \log_{10}(2) dB \approx 3.01 dB$ of extra squeezing is needed for each additional Bell pair. At sufficiently large squeezing and for large n_b , the success probability is approximately 0.5. The protocol can also be used to create a single Bell pair. In this case, with squeezing values readily achievable with current technology, the success probability is approximately 0.75, which is significantly higher than that achieved by protocols using photonic qubits and incomplete BSM. Note that the protocol proposed in Ref [14], which employs ancillary photonic qubits, also has a 0.75 theoretical success probability. For practical implementations with current technology, a key difference between the protocol in Ref. [14] and ours is that they employ photon-number-resolving measurements, whereas we rely on homodyne measurements.

which may prove to be more experimentally feasible.

Both proposed applications of our protocol, generating multiple Bell pairs per protocol iteration with a 0.5 success probability and generating a single Bell pair with a 0.75 probability, have the potential to significantly improve entanglement generation rates when implemented in a network. A direct comparison of the achievable improvement with that of previous protocols is of great interest. However, in addition to the EGP, the actual entanglement generation rate is influenced by optical fiber losses, various potential errors, and specific quantum repeaters and network protocols. We do not consider these effects here; the main goal of this paper is to introduce the protocol steps in an ideal scenario without losses. We plan to address loss and other realistic effects in future work.

The paper is organized as follows: Section II provides the necessary theoretical background. The CV and DV variables are introduced in Section II A, followed by a presentation of a pure CV entanglement swapping protocol in Section II B. The hybrid protocol is described in Section III. In Section III A, a detailed analytical and numerical investigation of the protocol with squeezed vacuum modes is presented. Potential limitations of the protocol, particularly those related to practical implementation in the near future, comparisons with other protocols, and the possible implementation of our protocol in a quantum repeater are discussed in Section IV. Finally, the summary and conclusions are outlined in Section V.

II. Preliminaries

A. CV and DV variables

Our protocol involves multi-qubit registers coupled to optical modes. In this section, we introduce the CV variables used to describe the optical modes and the DV variables used to describe the multi-qubit registers.

1. CV modes

Continuous modes are vectors belonging to the Hilbert space of square integrable functions, $L^2(\mathbb{R})$, usually represented in the continuous bases made up of the eigenvectors of the quadrature operators. The quadrature operators, denoted here by X and P, obey the canonical commutation relations [X, P] = i, and are characterized by continuous spectra

$$X|x\rangle = x|x\rangle \tag{1}$$

$$P|p\rangle = p|p\rangle, \qquad (2)$$

with $x, p \in \mathbb{R}$. The eigenvectors $\{|x\rangle\}$ and $\{|p\rangle\}$ are connected by the Fourier transform

$$|p\rangle = \frac{1}{\sqrt{2\pi}} \int_{-\infty}^{\infty} dx e^{ipx} |x\rangle. \tag{3}$$

2. Multi-qubit registers

A register of n qubits defines a finite 2^n -dimensional Hilbert space. This finite Hilbert space, together with the discrete quadrature operators introduced in this section, constitutes a model for the discretization of continuous modes.

The computational basis of the finite Hilbert space is formed by the vectors $\{|j\rangle\}_j$:

$$|j\rangle = |j_0\rangle |j_1\rangle \dots |j_{n-1}\rangle, \tag{4}$$

where $|j_q\rangle$ with $j_q \in \{0,1\}$ is the state of the qubit with index $q \in \{0,...,n-1\}$. The integer $j \in [0,2^n-1]$ is defined as the decimal representation of the binary number $j_0j_1...j_{n-1}$,

$$j = \sum_{q=0}^{n-1} j_q 2^{n-1-q}.$$
 (5)

We define the discrete quadrature operators acting on the n-qubit register such:

$$\bar{X} = -\sum_{q=0}^{n-1} \theta_q \sigma_q^z, \quad \text{with} \quad \theta_q = 2^{n-2-q} \Delta, \tag{6}$$

$$\bar{P} = \mathcal{F}\bar{X}\mathcal{F}^{-1},\tag{7}$$

where $\sigma_q^z = |0\rangle\langle 0|_q - |1\rangle\langle 1|_q$ is the Pauli σ^z operator acting on qubit q, Δ is the discretization interval defined as

$$\Delta = \sqrt{\frac{2\pi}{2^n}},\tag{8}$$

and \mathcal{F} is the quantum Fourier transform (QFT)

$$\mathcal{F} = \frac{1}{2^{\frac{n}{2}}} \sum_{j,k=0}^{2^{n}-1} e^{i\frac{2\pi}{2^{n}} \left(j - \frac{2^{n}-1}{2}\right) \left(k - \frac{2^{n}-1}{2}\right)} |k\rangle\langle j|. \tag{9}$$

The operator \bar{X} acts on the computational basis as

$$\bar{X}|j\rangle = \bar{x}_j|j\rangle$$
, with $\bar{x}_j = \left(j - \frac{2^n - 1}{2}\right)\Delta$. (10)

Thus, the computational basis vectors are eigenvectors of \bar{X} , with the eigenvalues forming a set of equidistant points $\{x_j\}_j$ separated by the interval Δ . Equation (10) is a discretized version of Eq. (1).

Moreover, the set $\{\mathcal{F}|j\rangle\}_j$ constitutes a basis for the discrete quadrature operator \bar{P} ,

$$\bar{P}(\mathcal{F}|j\rangle) = \bar{p}_j(\mathcal{F}|j\rangle), \text{ with } \bar{p}_j = \left(j - \frac{2^n - 1}{2}\right)\Delta,$$
 (11)

with the eigenvalues forming a set of equidistant points separated by the interval Δ . Equation (11) is the discretized version of Eq. (2), owing to the fact that the quantum Fourier transform \mathcal{F} (Eq. (9)) is the discretized version of the continuous Fourier transform defined by Eq. (3).

A detailed analysis of the discretization of the continuous modes and their representation on a finite Hilbert space is presented in [18, 19]. However, for the purpose of this paper, the definition of the discrete quadrature operators given by Eqs. (6) and (7) will suffice.

In analogy with the CV displacement operator, we introduce the discrete displacement operator here

$$\bar{D}(t) = e^{-it\Delta\bar{P}} |j\rangle = |(j+t) \bmod 2^n\rangle, \tag{12}$$

where t is an integer.

The main goal of the protocol is to produce Bell pairs shared between two separate registers, for example, one held by Alice and one held by Bob. Considering the Bell state $|\phi\rangle^+ = (|00\rangle_{AB} + |11\rangle_{AB})/\sqrt{2}$ and employing Eq. (4), the state of shared n Bell pairs is

$$|\phi(n)\rangle = \frac{1}{2^{\frac{n}{2}}} \left(\sum_{j_0 = 0, 1} |j_0 j_0\rangle_{AB} \right) \otimes \left(\sum_{j_1 = 0, 1} |j_1 j_1\rangle_{AB} \right) \otimes \dots \otimes \left(\sum_{j_{n-1} = 0, 1} |j_{n-1} j_{n-1}\rangle_{AB} \right) = \frac{1}{2^{\frac{n}{2}}} \sum_{j=0}^{2^{n} - 1} |jj\rangle_{AB}. \tag{13}$$

3. CV and DV coupling

The hybrid entanglement generation protocol requires a method to entangle the CV modes with the qubits. As described in the next section, our protocol employs the unitary

$$e^{-i\bar{X}\otimes X} = \prod_{q=0}^{n-1} e^{i\theta_q \sigma_q^z \otimes X},\tag{14}$$

where \bar{X} (see Eq. (6)) acts on n-qubit registers and X acts on the CV mode. The implementation of this unitary is shown in Fig. 1 and can be achieved by coupling the CV mode to each qubit independently, through an interaction

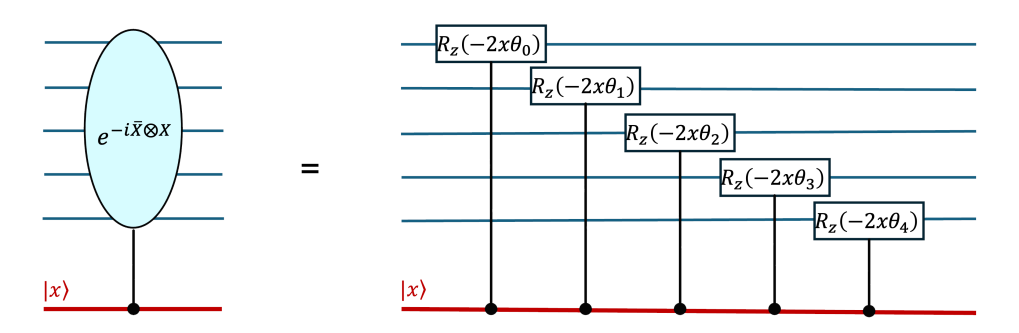


FIG. 1: Implementation of the unitary operator $e^{-i\bar{X}\otimes X}$ employed by our protocol. The blue lines represent a register of n qubits (in this example, n=5), and the red line represents a CV mode expressed in the continuous basis $\{|x\rangle\}$. According to Eq. (14), the implementation requires interaction $H_{int} \propto X\sigma_q^z$ between the CV mode and each qubit. It reduces to n conditional qubit phase rotations with angle $-2x\theta_q$ for $q\in\{0,\ldots,n-1\}$, where θ_q is defined in Eq. (6) and $R_z(\theta)=e^{-i\frac{\theta}{2}\sigma^z}$ is the single-qubit z-rotation.

proportional to the CV mode quadrature and a qubit Pauli operator. For example, an interaction Hamiltonian $H_{int} \propto X \sigma_q^x$, sandwiched between two single-qubit Hadamard gates H_q

$$e^{i\theta_q \sigma_q^z \otimes X} = H_q e^{i\theta_q \sigma_q^x \otimes X} H_q, \tag{15}$$

can be used to implement the unitary Eq. (14). This kind of interaction is realized, for instance, in systems with transmons coupled to a microwave cavity [20], or in systems with an electromagnetic mode coupled to qubits [21–23].

B. CV entanglement swapping protocol

Our hybrid protocol is a modified version of the entanglement swapping CV protocol described in [3]. We briefly outline the pure CV protocol below in a form slightly different from the original version, but more suitable for modification into our hybrid version (see also Appendix A for details). Since the purpose of this section is to establish a parallel between the CV protocol and the hybrid one, we will only consider the CV protocol in the nonphysical case that utilizes infinitely squeezed modes.

The CV protocol starts with Alice having two infinitely squeezed modes, 1 and 2,

$$|\chi\rangle_A = \int |x_1\rangle_A \, dx_1 \otimes \int |x_2\rangle_A \, dx_2. \tag{16}$$

Next, these two modes are entangled by a gate $e^{-X_1 \otimes X_2}$, where X_1 and X_2 are the quadrature operators for modes 1 and 2, respectively. At a separate location, Bob entangles modes 3 and 4 in the same way. Then Alice sends mode 2 and Bob sends mode 3 to Charlie. Charlie sends the two received modes through a 50:50 beam splitter and, afterwards, measures the quadrature X of one mode and the quadrature P of the other mode. The outcome of the measurement is sent through classical channels to Alice and Bob. Alice and Bob employ local operations that are dependent on the measurement results received from Charlie and obtain the entangled state

$$|\chi\rangle_{AB} = \int |x, x\rangle_{AB} \, dx. \tag{17}$$

Our hybrid protocol is inspired by the observation that the discretized version of Eq. (17) corresponds to an n-pair Bell state described by Eq. (13). Recall that the discretization of CV modes on n-qubit registers introduced in Section II A 2 maps the CV vector $|x\rangle$ to the n-qubit vector $|j\rangle$. Therefore, if we substitute the CV modes 1 and 4 with n-qubit states we expect the resulting state, in the limit of large n, to have a large overlap with an n-pair Bell state.

III. Hybrid CV-DV entanglement generation protocol

Our protocol describes a method for generating multiple Bell pairs between two distant nodes, each containing n qubits. The process begins by entangling the qubits at each node with a CV mode. The two CV modes are then

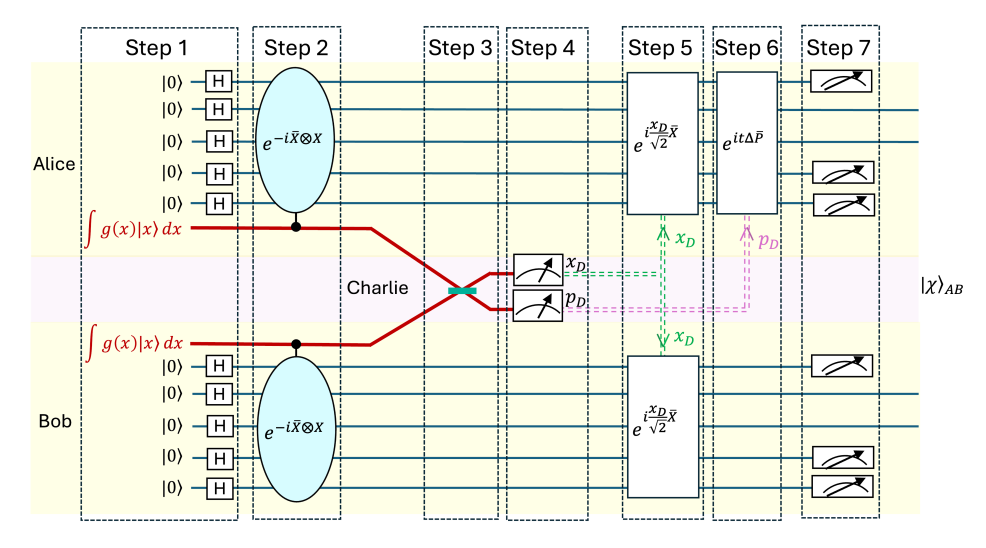


FIG. 2: Diagram of the hybrid CV-DV entanglement generation protocol. Step 1: Alice and Bob each start with an n-qubit register (blue solid lines, n=5 in this example) and a CV mode (red thick solid lines). A Hadamard gate H is applied to each qubit. The initial CV states are prepared in the quadrature basis as $\int g(x)|x\rangle dx$ (for squeezed vacuum, see Eq. (30)). Step 2: The n-qubit registers and the CV states are entangled locally through the operator $e^{-i\bar{X}\otimes X}$, defined by Eq. (14) and shown explicitly in Fig. 1. Step 3: The continuous modes are sent to Charlie, who passes them through a 50: 50 beam splitter. Step 4: Charlie measures the quadrature X of one mode and the quadrature P of the other and relays the measurement outcomes (denoted by x_D and p_D) to Alice and Bob via classical channels (dotted double lines). Step 5: Alice and Bob perform the local operations $e^{i\frac{\pi}{2}D}\bar{X}$, shown explicitly in Fig. 3a, on their qubit registers. Step 6: Alice performs the local operation $e^{it(p_D)\Delta\bar{P}}$, shown explicitly in Fig. 3b (see Eq. (28) for the definition of $t(p_D)$). Step 7: Alice and Bob measure their first qubit and their last s_c qubits (the choice of s_c is described in the text; in this example, $s_c=2$). The protocol is non-deterministic and succeeds when the final state $|\chi\rangle_{AB}$ approximates $n-1-s_c$ Bell pairs shared between Alice and Bob with the desired fidelity.

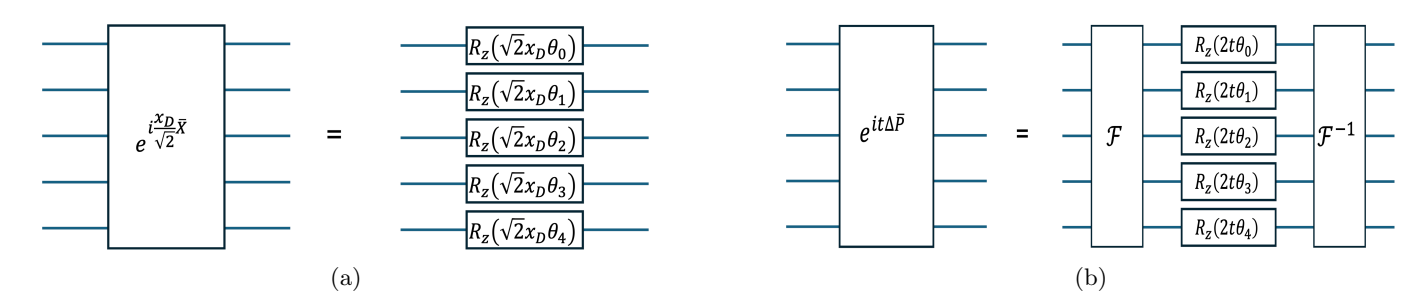


FIG. 3: a) The implementation of the operation $e^{i\frac{z_D}{\sqrt{2}}\bar{X}}$ on a register of n qubits reduces to n single-qubit z-rotations. b) The implementation of the operation $D(-t)=e^{it\Delta\bar{P}}$ on a register of n qubits reduces to n single-qubit z-rotations, sandwiched between a quantum Fourier transform \mathcal{F} and its inverse \mathcal{F}^{-1} . The value of θ_q , for $q \in \{0, 1, \ldots, n-1\}$ is given by Eq. (6). In this example n=5. The single-qubit z-rotation is defined as $R_z(\theta)=e^{-i\frac{\theta}{2}\sigma^z}$.

transmitted to a third location, where they pass through a 50:50 beam splitter, and their quadratures are measured using homodyne detection. The outcomes of the homodyne measurements determine the local operations to be subsequently performed at each node. Fidelity can be improved by measuring a subset of qubits in the computational basis. The protocol is non-deterministic, as its success depends on the outcomes of the homodyne and qubit measurements. In this section, a detailed explanation of the protocol steps is provided, along with an analysis of its success probability and fidelity.

The first part of the hybrid protocol is a straightforward modification of the CV protocol outlined in Section IIB and Appendix A. In the hybrid protocol, the continuous mode 1 at Alice and the continuous mode 4 at Bob are replaced by n-qubit registers. The n-qubit registers are treated as "discretized" continuous modes, as described

in Section II A 2. The protocol is illustrated in Fig. 2, and consists of the following steps:

1. Alice starts with an unentangled state consisting of a direct product between an n-qubit DV state and a CV mode:

$$|\chi\left(\text{step1}\right)\rangle_{A} = \left(\frac{1}{\sqrt{2^{n}}} \sum_{j=0}^{2^{n}-1} |j\rangle_{A}\right) \otimes \left(\int dx_{2}g(x_{2}) |x_{2}\rangle_{A}\right). \tag{18}$$

The DV initial state can be obtained by applying a single-qubit Hadamard gate to every qubit initially prepared in the state $|0\rangle$. Similarly Bob starts with a product of a CV mode and a n-qubit DV state:

$$|\chi\left(\text{step1}\right)\rangle_{B} = \left(\int dx_{3}g(x_{3})|x_{3}\rangle_{B}\right) \otimes \left(\frac{1}{\sqrt{2^{n}}} \sum_{k=0}^{2^{n}-1} |k\rangle_{B}\right). \tag{19}$$

The initial CV modes are defined by the function g(x), with the normalization condition $\int |g(x)|^2 dx = 1$.

2. Alice and Bob entangle their CV and DV modes by applying the local operator $e^{-i\bar{X}\otimes X}$ (see Eqs. (10) and (14)):

$$|\chi \text{ (step 2)}\rangle_A = \frac{1}{\sqrt{2^n}} \sum_{j=0}^{2^n - 1} \int dx_2 g(x_2) e^{-i\bar{x}_j x_2} |j, x_2\rangle_A,$$
 (20)

$$|\chi \text{ (step 2)}\rangle_B = \frac{1}{\sqrt{2^n}} \sum_{k=0}^{2^n - 1} \int dx_3 g(x_3) e^{-i\bar{x}_k x_3} |x_3, k\rangle_B.$$
 (21)

3. Alice and Bob send their continuous modes to Charlie. Charlie sends them through a 50:50 beam splitter,

$$|\chi \text{ (step 3)}\rangle_{ABC} = \frac{1}{2^n} \sum_{i,k=0}^{2^n - 1} \int dx_2 dx_3 g(x_2) g(x_3) e^{-i\bar{x}_j x_2} e^{-ix_3 \bar{x}_k} |j,k\rangle_{AB} \left| \frac{x_2 + x_3}{\sqrt{2}}, \frac{-x_2 + x_3}{\sqrt{2}} \right\rangle_C. \tag{22}$$

4. Employing homodyne measurement, Charlie measures the quadrature X for one mode and the quadrature P for the other mode. By denoting the results of the measurement by x_D and p_D , the state becomes (see Appendix B):

$$|\chi \text{ (step 4)}\rangle_{AB} = \frac{1}{2^n \sqrt{P(x_D, p_D)}} \sum_{j,k=0}^{2^n - 1} e^{-ix_D \frac{\bar{x}_j + \bar{x}_k}{\sqrt{2}}} \hat{h}_{x_D} \left(p_D - \frac{\bar{x}_j - \bar{x}_k}{\sqrt{2}} \right) |j, k\rangle_{AB},$$
 (23)

where

$$\hat{h}_{x_D}(p) = \frac{1}{\sqrt{2\pi}} \int dx g\left(\frac{x_D + x}{\sqrt{2}}\right) g\left(\frac{x_D - x}{\sqrt{2}}\right) e^{ixp},\tag{24}$$

and the probability to measure x_D and p_D is

$$P(x_D, p_D) = \frac{1}{2^{2n}} \sum_{j,k=0}^{2^n - 1} \left| \hat{h}_{x_D} \left(p_D - \frac{\bar{x}_j - \bar{x}_k}{\sqrt{2}} \right) \right|^2.$$
 (25)

Charlie sends the values of x_D and p_D to Alice and Bob through classical channels.

5. Alice and Bob apply the operator $e^{i\frac{x_D}{\sqrt{2}}\bar{X}}$ to their discrete mode,

$$|\chi \text{ (step5)}\rangle_{AB} = \frac{1}{2^n \sqrt{P(x_D, p_D)}} \sum_{j,k=0}^{2^n - 1} \hat{h}_{x_D} \left(p_D - \frac{\bar{x}_j - \bar{x}_k}{\sqrt{2}} \right) |j, k\rangle_{AB}.$$
 (26)

Since the operator \bar{X} is defined as a linear combination of Pauli σ_q^z operators (see Eq. (6)), the implementation of $e^{i\frac{x_D}{\sqrt{2}}\bar{X}}$ operation on a DV register reduces to n single-qubit R_z rotations, one on each qubit, as illustrated in Fig. 3a (see Appendix D in [19] for the explicit implementation).

6. Alice applies the discrete displacement operator $\bar{D}(-t)$,

$$|\chi\rangle_{AB} = |\chi \text{ (step 6)}\rangle_{AB} = \frac{1}{2^n \sqrt{P(x_D, p_D)}} \sum_{j,k=0}^{2^n - 1} \hat{h}_{x_D} \left(p_D - \frac{\bar{x}_j - \bar{x}_k}{\sqrt{2}} \right) |(j - t) \mod 2^n, k\rangle_{AB},$$
 (27)

where the integer parameter t is defined such that

$$\sqrt{2}p_D = (t + \delta_p)\Delta, \text{ with } -0.5 < \delta_p \le 0.5 \text{ and } t \in \mathbb{Z}.$$
(28)

Both the integer $t(p_D)$ and the real $\delta_p(p_D)$ are uniquely determined by the measurement outcome p_D . The implementation of $D(-t) = e^{it\Delta\bar{P}} = \mathcal{F}e^{it\Delta\bar{X}}\mathcal{F}^{-1}$ (see Eqs. (7) and (12)) requires single-qubit R_z rotations sandwiched between two quantum Fourier transform (QFT) operations, as illustrated in Fig. 3b (see Appendix C in [19] for the explicit implementation).

7. This final step involves measurement of qubits in the computational basis, and can be considered a purification process. At this step Alice and Bob measure the first qubit and the last s_c qubits of their registers. The resulting state is a $2 \times n_b$ qubit state, with $n_b = n - 1 - s_c$. The fidelity of the protocol is

$$F_{n_b} = \left| \left\langle \chi | \phi(n_b) \right\rangle \right|^2, \tag{29}$$

where $|\phi(n_b)\rangle$ is the n_b -pair Bell state defined by Eq. (13) on the qubits $\{1, \ldots, n-1-s_c\}$ of both Alice and Bob. The number of qubits necessary to be measured (equal to $1+s_c$) depends on the wavefunction of the initial CV modes (for example, on the squeezing strength when the wavefunction is Gaussian), the size n of the qubit registers, and the desired protocol fidelity. The success of the protocol is probabilistic and depends on the value of the homodyne measurements (x_D and p_D) and on the outcome of the measured qubits.

This last step of our protocol will be described at length in Section III A for the case when the initial wavefunction g(x) is Gaussian.

A. Entanglement generation with squeezed vacuum

The details of the last step (step 7) of the hybrid protocol depend on the CV wavefunction. Here we will present the case with initial Gaussian CV modes,

$$g(x) = \pi^{-\frac{1}{4}} \frac{1}{\sqrt{\sigma}} e^{-\frac{x^2}{2\sigma^2}}.$$
 (30)

The Gaussian wavefunctions describe squeezed vacuum states, with the standard deviation σ related to the squeezing factor through the relation $\sigma = e^{-r}$ [24]. In our units, $\sigma = 1$ corresponds to the vacuum state. Our protocol requires $\sigma > 1$ (i.e. r < 0) which corresponds to the squeezing of the P quadrature.

Employing Eqs. (24) and (30) we obtain,

$$\hat{h}_{x_D}(p) = \frac{1}{\sqrt{\pi}} e^{-\frac{x_D^2}{2\sigma^2}} e^{-\frac{p^2\sigma^2}{2}}.$$
(31)

Equation (25) yields the probability to measure x_D and p_D ,

$$P(x_D, p_D) = P(x_D) P(p_D)$$
(32)

where

$$P(x_D) = \frac{1}{\sigma\sqrt{\pi}}e^{-\frac{x_D^2}{\sigma^2}},\tag{33}$$

and

$$P(p_D) = \frac{1}{2^{2n}} \sum_{j,k=0}^{2^n - 1} \left| u \left(p_D - \frac{\bar{x}_j - \bar{x}_k}{\sqrt{2}} \right) \right|^2, \tag{34}$$

with

$$u(p) = \sqrt{\frac{\sigma}{\sqrt{\pi}}} e^{-\frac{\sigma^2}{2}p^2}.$$
 (35)

The measurement probabilities of the two quadratures, x_D and p_D , are independent of each other for Gaussian modes. This is not necessarily true for other choices of g(x).

For Gaussian modes the state given by Eq. (27) is independent of the outcome x_D , and can be written as

$$|\chi\rangle_{AB} = \frac{1}{\sqrt{P(p_D)}} \frac{1}{2^n} \sum_{j,k=0}^{2^n - 1} u\left(p_D - \frac{\bar{x}_j - \bar{x}_k}{\sqrt{2}}\right) |(j-t) \bmod 2^n, k\rangle_{AB}.$$
 (36)

The purification step of the protocol can be understood by analyzing the following approximation. For a given σ , there is a positive dimensionless cutoff parameter c such that $u(p) \approx 0$ when $|p| \sigma > c$. In the following analytical expressions, we will neglect u(p) for $|p| > \frac{c}{\sigma}$. We keep c as a parameter to control this truncation error. Increasing the value of c decreases the truncation errors exponentially. As discussed in Section III A 3, the truncation errors are related to the protocol fidelity. Numerically, we find that $c \gtrsim 2.2$ yields fidelity errors $\lesssim 1\%$ for our protocol.

The truncation of u(p) implies that in Eq. (36) we can write

$$u\left(p_D - \frac{\bar{x}_j - \bar{x}_k}{\sqrt{2}}\right) \equiv u\left[\left(t - j + k + \delta_p\right)\frac{\Delta}{\sqrt{2}}\right] \approx \sum_{m = -m_c}^{m_c} u\left[\left(m + \delta_p\right)\frac{\Delta}{\sqrt{2}}\right] \delta_{j-t,k-m},\tag{37}$$

where t and δ_p are defined by Eq. (28), \bar{x}_j and \bar{x}_k by Eq. (10), and m_c can be any positive integer such that

$$\left(m_c + \frac{1}{2}\right) \frac{\Delta}{\sqrt{2}}\sigma > c.
\tag{38}$$

It is convenient to replace m_c with $2^{s_c} - 1$ in Eq. (37), where the parameter s_c is a positive integer such that $2^{s_c} - 1 \ge m_c$. Equation (38) implies that s_c should be chosen such that

$$\left(2^{s_c} - \frac{1}{2}\right)\sqrt{\frac{\pi}{2^n}}\sigma > c.$$
(39)

Finally, employing the truncation described by Eq. (37), the wavefunction described by Eq. (36) becomes

$$|\chi\rangle_{AB} \approx \frac{1}{2^n \sqrt{P(p_D)}} \sum_{m=-2^{s_c}+1}^{2^{s_c}-1} u \left[(m+\delta_p) \frac{\Delta}{\sqrt{2}} \right] \sum_{k=\max(0,m-t)}^{2^n-1-\min(0,m-t)} |(k-m) \bmod 2^n, k\rangle_{AB}.$$
 (40)

1. Purification step

The purification step of our protocol requires the measurement of the first qubit (indexed by 0 in our notation, see Eq. (4)) and the last s_c qubits (indexed by $\{n - s_c, \dots, n - 1\}$) at each register. In total each of Alice and Bob measures and discards $1 + s_c$ qubits. Consequently, the total number of Bell pairs for successful protocols will be

$$n_b = n - 1 - s_c. (41)$$

The optimal value of s_c for our protocol, which depends on the fidelity, the squeezing σ and the registers' size n, will be discussed in Section III A 3.

We begin by analyzing the measurement of the last qubit in Alice's and Bob's registers, indexed as n-1 in our notation. If the measured values of this qubit at Alice and Bob are different, the protocol is considered unsuccessful. If the measured values are the same, *i.e.*, either both 0 or both 1, the post-measurement state is obtained by applying the projector operators:

$$P_{0_{n-1}0_{n-1}} = \mathbb{I}_{2\times(n-1)} \otimes |0_{n-1}0_{n-1}\rangle\langle 0_{n-1}0_{n-1}| \tag{42}$$

or

$$P_{1_{n-1}1_{n-1}} = \mathbb{I}_{2\times(n-1)} \otimes |1_{n-1}1_{n-1}\rangle\langle 1_{n-1}1_{n-1}|, \tag{43}$$

respectively.

In order to calculate how these operators act on the state described by Eq. (40), we used the fact that an n-qubit integer k (see Eq. (5)) can be written as

$$k = \sum_{q=0}^{n-2} k_q 2^{n-1-q} + k_{n-1} = 2 \sum_{q=0}^{n'-1} k_q 2^{n'-1-q} + k_{n-1} = 2k' + k_{n-1},$$
(44)

where k' is the decimal representation of the state encoded in the first n' = n - 1 qubits. Then, for even m = 2m' and even k = 2k' we have,

$$P_{0_{n-1}0_{n-1}} \left| (2k' - 2m') \bmod 2^n, 2k' \right\rangle_{AB} = \left| (k' - m') \bmod 2^{n'}, k' \right\rangle_{AB} \otimes \left| 0_{n-1}0_{n-1} \right\rangle_{AB}, \tag{45}$$

$$P_{1_{n-1}1_{n-1}} | (2k' - 2m') \bmod 2^n, 2k' \rangle_{AB} = 0, \tag{46}$$

for even m = 2m' and odd k = 2k' + 1,

$$P_{0_{n-1}0_{n-1}} | (2k'+1-2m') \bmod 2^n, 2k'+1 \rangle_{AB} = 0, \tag{47}$$

$$P_{1_{n-1}1_{n-1}} \left| (2k' + 1 - 2m') \bmod 2^n, 2k' + 1 \right\rangle_{AB} = \left| (k' - m') \bmod 2^{n'}, k' \right\rangle_{AB} \otimes \left| 1_{n-1}1_{n-1} \right\rangle_{AB}, \tag{48}$$

while for odd m and any k,

$$P_{0_{n-1}0_{n-1}} | (k-m) \bmod 2^n, k \rangle_{AB} = P_{1_{n-1}1_{n-1}} | (k-m) \bmod 2^n, k \rangle_{AB} = 0.$$

$$(49)$$

Employing Eqs. (45)–(49), the unnormalized wavefunction described by Eq. (40) becomes, after the measurement,

$$P_{0_{n-1}0_{n-1}} |\chi\rangle_{AB} = \frac{1}{\sqrt{P(p_D)}} \frac{1}{2^n} \sum_{m'=-2^{s_C-1}+1}^{2^{s_C-1}-1} u \left[(2m' + \delta_p) \frac{\Delta}{\sqrt{2}} \right] \times$$

$$\times \sum_{k'=\max(0,m'-\lfloor \frac{t}{2} \rfloor)} |(k'-m') \bmod 2^{n-1}, k'\rangle_{AB} \otimes |0_{n-1}0_{n-1}\rangle_{AB},$$
(50)

when the value of measured qubits at both Alice and Bob is 0, or

$$P_{1_{n-1}1_{n-1}} |\chi\rangle_{AB} = \frac{1}{\sqrt{P(p_D)}} \frac{1}{2^n} \sum_{m'=-2^{s_c-1}+1}^{2^{s_c-1}-1} u \left[(2m' + \delta_p) \frac{\Delta}{\sqrt{2}} \right] \times$$

$$\times \sum_{k'=\max(0,m'-\lceil \frac{t}{2} \rceil)} |(k'-m') \bmod 2^{n-1}, k'\rangle_{AB} \otimes |1_{n'}1_{n-1}\rangle_{AB},$$
(51)

when the value of measured qubits is 1. In Eqs. (50) and (51), $\left| (k'-m') \bmod 2^{n'}, k' \right\rangle_{AB}$ is a state stored on the first n-1 qubits of Alice and the first n-1 qubits of Bob. The limits of the summation over the k' in Eq. (50) involves the floor integer $\lfloor \frac{t}{2} \rfloor$, which rounds down $\frac{t}{2}$ (see Eq. (57)), while in Eq. (51) it involves the ceiling integer $\lceil \frac{t}{2} \rceil$, which rounds up $\frac{t}{2}$ (see Eq. (58)).

Equations (50) and (51) can be generalized to describe the state after the measurement of all s_c qubits indexed by $n - s_c, \ldots, n - 1$, in Alice's and Bob's registers. The protocol is considered unsuccessful when the outcome at Alice is not identical to the outcome at Bob. When the outcomes are identical, they determine a sequence of s_c values of 0 and 1,

$$S = \{j_{n-s_c}, \dots, j_{n-2}, j_{n-1}\},\tag{52}$$

where j_q is the outcome of the measurement of the qubit indexed by q at both Alice's and Bob's locations. The unnormalized post-measurement state is given by

$$P_S |\chi\rangle_{AB} = \frac{1}{2^n \sqrt{P(p_D)}} u \left(\delta_p \frac{\Delta}{\sqrt{2}}\right) \times \sum_{k=\max(0,-t_S)}^{2^{n-s_c}-1+\min(0,-t_S)} |k,k\rangle_{AB} \otimes |S\rangle_{AB},$$
 (53)

where

$$|S\rangle_{AB} = |j_{n-s_c}j_{n-s_c}\rangle_{AB} \otimes \cdots \otimes |j_{n-1}j_{n-1}\rangle_{AB}, \qquad (54)$$

$$P_S = \mathbb{I}_{2 \times (n - s_c)} \otimes |S\rangle\langle S|, \tag{55}$$

and $|k,k\rangle_{AB}$ is a state spanned by the first $n-s_c$ qubits at Alice and by the first $n-s_c$ qubits at Bob. The integer t_S is defined by

$$t_S = \left[\dots \left[\left[t \times \frac{1}{2} \right]_{j_{n-1}} \times \frac{1}{2} \right]_{j_{n-2}} \dots \times \frac{1}{2} \right]_{j_{n-s_c}}, \tag{56}$$

where we denote

$$[x]_0 \equiv \lfloor x \rfloor \equiv \text{ floor function}(x) \equiv \max\{n \in \mathbb{Z} | n \le x\}$$
 (57)

$$[x]_0 \equiv \lfloor x \rfloor \equiv \text{ floor function}(x) \equiv \max\{n \in \mathbb{Z} | n \le x\}$$
 (57)
$$[x]_1 \equiv \lceil x \rceil \equiv \text{ ceiling function}(x) \equiv \min\{n \in \mathbb{Z} | n \ge x\}.$$
 (58)

Now we will analyze the measurement of the first qubit, indexed by 0, in Alice's and Bob's registers. We start by imposing the following requirement: the protocol is considered successful only when

$$p_D \in \left(-(2^n+1)\frac{\Delta}{2\sqrt{2}}, (2^n+1)\frac{\Delta}{2\sqrt{2}}\right] \iff t \in \left[-2^{n-1}, 2^{n-1}\right].$$
 (59)

In the event that the homodyne measurement performed by Charlie yields a value of p_D outside of this range, the protocol is abandoned. Equation (59) implies $|t_S| \leq 2^{n-s_c-1}$, where t_S was defined by Eq. (56). Therefore, for a successful protocol, the state described by Eq. (53) can be written as

$$|\chi\rangle_{AB} = \frac{1}{2^n \sqrt{P(p_D)P(S)}} u\left(\delta_p \frac{\Delta}{\sqrt{2}}\right) \left[\sum_{k=\max(0,-t_S)}^{2^{n-s_c-1}-1} |k,k\rangle_{AB} + \sum_{k=2^{n-s_c-1}}^{2^{n-s_c}-1+\min(0,-t_S)} |k,k\rangle_{AB}\right] \otimes |S\rangle_{AB}, \quad (60)$$

where P(S) is a normalization constant equal to the probability of the measurement of the $2 \times s_c$ qubits yielding the sequence S at both Alice and Bob locations. Since

$$\sum_{k=0}^{2^{n-s_c-1}-1} |k,k\rangle_{AB} = 2^{\frac{n-s_c-1}{2}} |0_00_0\rangle_{AB} \otimes |\phi(n-1-s_c)\rangle,$$
(61)

and

$$\sum_{k=2^{n-s_c-1}}^{2^{n-s_c}-1} |k,k\rangle_{AB} = 2^{\frac{n-s_c-1}{2}} |1_0 1_0\rangle_{AB} \otimes |\phi(n-1-s_c)\rangle,$$
(62)

Eq. (60) reads

$$|\chi\rangle_{AB} = \frac{1}{2^n \sqrt{P(p_D)P(S)}} u\left(\delta_p \frac{\Delta}{\sqrt{2}}\right) \tag{63}$$

$$\times \left\{ \begin{array}{l} \left[2^{\frac{n-s_{c}-1}{2}} \left| 0_{0}0_{0} \right\rangle_{AB} \otimes \left| \phi(n-1-s_{c}) \right\rangle + \sum_{k=2^{n-s_{c}}-t}^{2^{n-s_{c}}-t_{S}-1} \left| k, k \right\rangle \right] \otimes \left| S \right\rangle_{AB} & \text{if } t \in \left(0, 2^{n-1}\right] \\ 2^{\frac{n-s_{c}-1}{2}} \left(\left| 0_{0}0_{0} \right\rangle_{AB} + \left| 1_{0}1_{0} \right\rangle_{AB} \right) \otimes \left| \phi(n-1-s_{c}) \right\rangle \otimes \left| S \right\rangle_{AB} = 2^{\frac{n-s_{c}}{2}} \left| \phi(n-s_{c}) \right\rangle \otimes \left| S \right\rangle_{AB} & \text{if } t = 0 \\ \left[\sum_{k=-t_{S}}^{2^{n-s_{c}-1}-1} \left| k, k \right\rangle + 2^{\frac{n-s_{c}-1}{2}} \left| 1_{0}1_{0} \right\rangle_{AB} \otimes \left| \phi(n-s_{c}-1) \right\rangle \right] \otimes \left| S \right\rangle_{AB} & \text{if } t \in \left[-2^{n-1}, 0 \right) \end{array} \right.$$

Equation (63) shows that the outcome of the measurement of the first qubit should be correlated with the outcome of the homodyne measurement for a successful protocol. Thus, when the homodyne measurement yields a value of p_D that implies $t \in (0, 2^{n-1}]$, the protocol is considered successful if the outcome of the first qubit measurement is 0 at both Alice's and Bob's locations. For $t \in [-2^{n-1}, 0)$, the protocol is successful if the first qubit measurement yields 1

at both Alice's and Bob's locations. When t = 0, the protocol is successful if the outcome of first qubit measurement at Alice's and Bob's is the same, either both 0 or both 1.

To summarize, the purification step for a protocol with Gaussian CV modes consists of the measurement of qubit 0 and qubits $n-s_c,\ldots,n-1$ of Alice's and Bob's registers. The protocol is successful when both propositions i) and ii) are simultaneously true, where the proposition i) is "the outcome of the measurement of the $1+s_c$ qubits at Alice is the same as the outcome at Bob" and the proposition ii) is "the first qubit is 0 and $t(p_d) \in \left[0, 2^{n-1}\right]$, or, the first qubit is 1 and $t(p_d) \in \left[-2^{n-1}, 0\right]$ ".

2. Success probability for high-fidelity protocols

The infidelity of our protocol is of the order of the truncation error introduced by Eq. (37). For sufficiently large s_c , these truncation errors are negligible and the protocol yields n_b Bell pairs with high-fidelity when the measurement outcomes satisfy the conditions summarized at the end of Section III A 1. Employing Eq. (63), the conditional probability to produce n_b Bell pairs for a successful measurement outcome is:

$$P\left(\phi(n-s_{c}-1) \mid j_{0,A}, j_{n-s_{c},A}, \dots, j_{n-1,A} = j_{0,B}, j_{n-s_{c},B}, \dots, j_{n-1,B} = \{0,S\}, p_{D} \in \left(-\frac{\Delta}{2\sqrt{2}}, (2^{n}+1)\frac{\Delta}{2\sqrt{2}}\right]\right) = \begin{pmatrix} \phi(n-s_{c}-1) \mid j_{0,A}, j_{n-s_{c},A}, \dots, j_{n-1,A} = j_{0,B}, j_{n-s_{c},B}, \dots, j_{n-1,B} = \{1,S\}, p_{D} \in \left(-(2^{n}+1)\frac{\Delta}{2\sqrt{2}}, \frac{\Delta}{2\sqrt{2}}\right] \end{pmatrix} = \begin{pmatrix} 1 \\ 2^{n+1+s_{c}}P(p_{D})P(S) \end{pmatrix} u \left[\delta_{p}\left(p_{D}\right)\frac{\Delta}{\sqrt{2}}\right]^{2},$$

where $j_{q,A}$ $(j_{q,B})$ denotes the outcome of the measurement of qubit q in Alice's (Bob's) register and S is defined by Eq. (52).

Consequently, the protocol probability of producing n_b Bell pairs is given by

$$P\left[\phi(n-s_{c}-1)\right] = \int_{-(2^{n-1}+1)\frac{\Delta}{2\sqrt{2}}}^{\frac{\Delta}{2\sqrt{2}}} P(p_{D}) \sum_{S} P(S) \frac{1}{2^{n+1+s_{c}} P(p_{D}) P(S)} u \left[\delta_{p}\left(p_{D}\right) \frac{\Delta}{\sqrt{2}}\right]^{2} dp_{D}$$

$$+ \int_{-\frac{\Delta}{2\sqrt{2}}}^{(2^{n-1}+1)\frac{\Delta}{2\sqrt{2}}} P(p_{D}) \sum_{S} P(S) \frac{1}{2^{n+1+s_{c}} P(p_{D}) P(S)} u \left[\delta_{p}\left(p_{D}\right) \frac{\Delta}{\sqrt{2}}\right]^{2} dp_{D}$$

$$= \frac{1}{2^{n+1}} \left(\sum_{t=-2^{n-1}}^{-1} +2 + \sum_{t=1}^{2^{n-1}}\right) \int_{-\frac{\Delta}{2\sqrt{2}}}^{\frac{\Delta}{2\sqrt{2}}} |u\left(p\right)|^{2} dp = \left(\frac{1}{2} + \frac{1}{2^{n}}\right) \operatorname{erf}\left(\frac{\sigma}{2}\sqrt{\frac{\pi}{2^{n}}}\right).$$

$$(65)$$

To derive Eq. (65) we used $\sum_{S} = 2^{s_c}$ and

$$\int_{-\frac{\Delta}{2\sqrt{2}}}^{\frac{\Delta}{2\sqrt{2}}} |u(p)|^2 dp = \frac{\sigma}{\sqrt{\pi}} \int_{-\frac{\Delta}{2\sqrt{2}}}^{\frac{\Delta}{2\sqrt{2}}} dp e^{-\sigma^2 p^2} = \operatorname{erf}\left(\frac{\sigma}{2}\sqrt{\frac{\pi}{2^n}}\right),\tag{66}$$

where erf() is the error function.

By inspecting Eq. (63), one can see that when the homodyne measurement yields t = 0, the resulting state consists of $n - s_c$ Bell pairs, *i.e.* the protocol produces one extra Bell pair compared to the case $t \neq 0$. The probability of our protocol producing $n - s_c$ Bell pairs is

$$P\left[\phi(n-s_c)\right] = \int_{-\frac{\Delta}{2\sqrt{2}}}^{\frac{\Delta}{2\sqrt{2}}} P(p_D) \sum_{S} P(S) \frac{1}{2^{n+s_c} P(p_D) P(S)} \left| u\left[\delta_p\left(p_D\right) \frac{\Delta}{\sqrt{2}}\right] \right|^2 dp_D = \frac{1}{2^n} \operatorname{erf}\left(\frac{\sigma}{2} \sqrt{\frac{\pi}{2^n}}\right). \tag{67}$$

Since having $n - s_c$ Bell pairs automatically implies having $n - s_c - 1$ Bell pairs, a term equal to $P[\phi(n - s_c)]$ is also included in $P[\phi(n - s_c - 1)]$, as can be seen in Eq. (65).

The probability to create $n-s_c$ Bell pairs is small for large n. However, for small n, this probability has a significant contribution to the success probability of the protocol. For example, when n=2, $s_c=0$ and the squeezing is large enough, this contribution is ≈ 0.25 , bringing the success probability for creating a single Bell pair up to ≈ 0.75 (see discussion in Section III A 3).

3. Protocol efficiency and fidelity

In this section, we investigate the success probability and fidelity of the protocol and calculate the optimal value of s_c . The protocol is considered successful if fidelity is greater than a desired threshold. According to this definition, the success probability is a function of the fidelity threshold.

The purification step described in Section III A 1 was justified for a choice of s_c large enough to ensure that the truncation errors in Eq. (37) are small. This condition is met when s_c satisfies Eq. (39), which implies that

$$s_c \ge \tilde{s}(\sigma, n_b) = 2\log_2\left(\frac{c}{\sigma}\sqrt{\frac{2^{n_b}}{\pi}} + \sqrt{\frac{2^{n_b}c^2}{\pi\sigma^2} + 1}\right) - 1.$$
 (68)

When the truncation errors are negligibly small, the success probability of a protocol with σ , n_b and s_c is given by (see Eq. (65)),

$$P(\sigma, s_c, n_b) = \left(\frac{1}{2} + \frac{1}{2^{n_b} 2^{s_c+1}}\right) \operatorname{erf}\left(\frac{\sigma}{\sqrt{2^{s_c+1}}} \sqrt{\frac{\pi}{2^{n_b+2}}}\right),\tag{69}$$

and is monotonically decreasing with increasing s_c . This implies that the maximum probability to produce n_b Bell pairs at a fixed σ is attained for the minimum integer s_c satisfying Eq. (68), *i.e.* when

$$s_c(\sigma, n_b) = \lceil 2 \log_2 \left(\frac{c}{\sigma} \sqrt{\frac{2^{n_b}}{\pi}} + \sqrt{\frac{2^{n_b} c^2}{\pi \sigma^2} + 1} \right) \rceil - 1.$$
 (70)

Since $s_c(\sigma, n_b)$ takes integer values, it exhibits a descending stair-step behavior as a function of increasing σ , jumping from the value s_c to $s_c - 1$ when

$$\sigma = \sigma_c \equiv \frac{2c}{(2^{s_c+1} - 1)} \sqrt{\frac{2^{n_b + s_c + 1}}{\pi}}.$$
 (71)

The maximum success probability is obtained by replacing s_c in Eq. (69) with $s_c(\sigma, n_b)$ given by Eq. (70),

$$P(\sigma, n_b) = P(\sigma, s_c, n_b)|_{s_c = s_c(\sigma, n_b)}.$$
(72)

The discontinuity of $s_c(\sigma, n_b)$ manifests as a discontinuity in $P(\sigma, n_b)$ as a function of σ , for values of σ that satisfy Eq. (71). Notice that $s_c(\sigma, n_b)$ and $P(\sigma, n_b)$ depend implicitly on the fidelity threshold since they depend on the cutoff parameter c, and c exerts strong influence on the fidelity.

To analyze the efficiency of our protocol for large n_b it is useful to determine analytical bounds for the maximum success probability,

$$P_{lower}\left(\sigma, n_{b}\right) < P\left(\sigma, n_{b}\right) \le P_{upper}\left(\sigma, n_{b}\right). \tag{73}$$

Employing Eq. (68) we find

$$P_{upper}\left(\sigma, n_{b}\right) = \left(\frac{1}{2} + \frac{1}{2^{n_{b}}} \frac{\pi\sigma^{2}}{\left(c\sqrt{2^{n_{b}}} + \sqrt{2^{n_{b}}c^{2} + \pi\sigma^{2}}\right)^{2}}\right) \operatorname{erf}\left(\frac{\pi\sigma^{2}}{2\sqrt{2^{n_{b}}}\left(c\sqrt{2^{n_{b}}} + \sqrt{2^{n_{b}}c^{2} + \pi\sigma^{2}}\right)}\right),\tag{74}$$

while the relation $s_c < \tilde{s}(\sigma, n_b) + 1$ (implied by Eqs. (68) and (70)) yields

$$P_{lower}(\sigma, n_b) = \left(\frac{1}{2} + \frac{1}{2^{n_b+1}} \frac{\pi \sigma^2}{\left(c\sqrt{2^{n_b}} + \sqrt{2^{n_b}c^2 + \pi\sigma^2}\right)^2}\right) \operatorname{erf}\left(\frac{\pi \sigma^2}{2\sqrt{2^{n_b+1}}\left(c\sqrt{2^{n_b}} + \sqrt{2^{n_b}c^2 + \pi\sigma^2}\right)}\right). \tag{75}$$

As can be inferred from Eq. (65), the success probability increases with $\sigma/\sqrt{2^n}$, reaching the maximum value of $\approx 0.5 + 0.5^n$ for large squeezing factors (i.e. large σ). However, squeezing is a technologically expensive resource, with the maximum squeezing achieved with current technology being 15dB [25]. The present technological limitation of the squeezing factor restricts the number of Bell pairs that can be produced by our protocol.

For a fixed success probability, the minimum squeezing necessary to produce n_b Bell pairs, expressed in decibels, is proportional to n_b , with a slope of approximately 3.01dB per Bell pair. The minimum squeezing necessary to produce

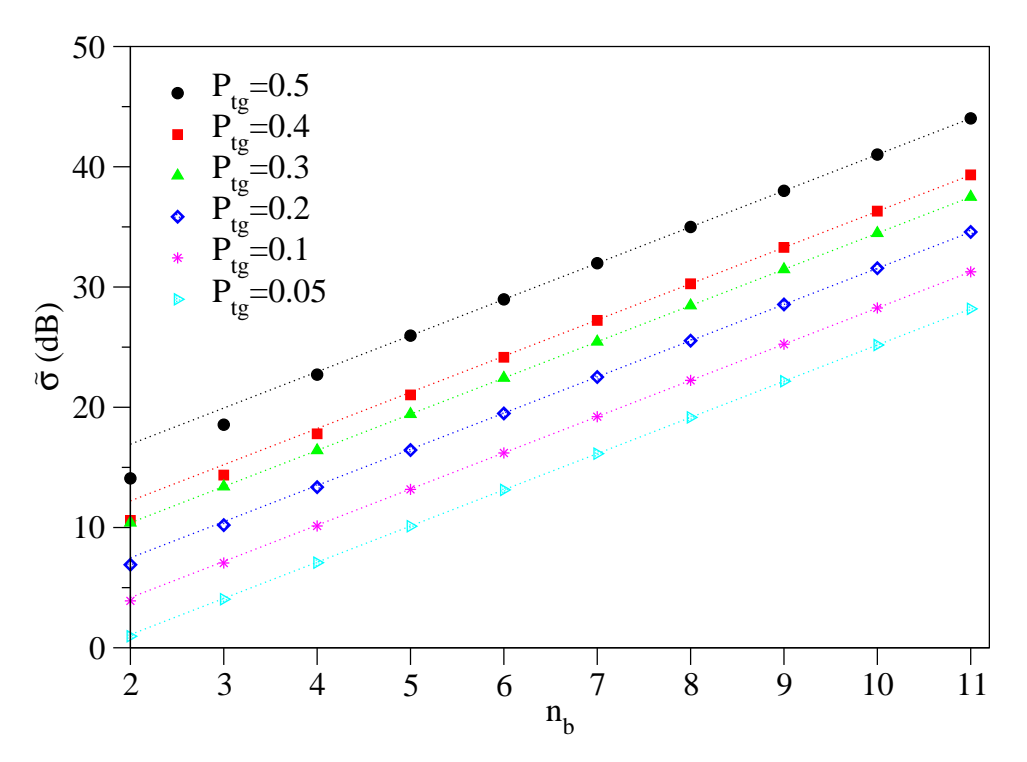


FIG. 4: The squeezing parameter $\tilde{\sigma}(dB)$ necessary to produce n_b Bell pairs for different target probabilities of success, plotted against n_b . The calculations use a cutoff parameter c = 2.2, ensuring a fidelity F > 0.99. The dependence is linear for large n_b , with a slope of approximately 3.01dB per Bell pair, as predicted by Eq. (78).

 n_b Bell pairs can be calculated by solving $P(\sigma, n_b) = P_{tg}$, where P_{tg} is the target success probability and $P(\sigma, n_b)$ is given by Eq. (72). The solutions, obtained numerically, are illustrated in Fig. 4, where $\tilde{\sigma}(dB)$ is defined as:

$$\tilde{\sigma}(dB) \equiv 20 \log_{10}(\sigma).$$
 (76)

The linear dependence of $\tilde{\sigma}$ versus n_b can be understood by inspecting Eqs. (74) and (75). Ignoring the term proportional to $\frac{1}{2^{n_b}}$ (which becomes small for large n), we can approximate:

$$P_{upper,lower}\left(\sqrt{2}\sigma, n_b + 1\right) \approx P_{upper,lower}\left(\sigma, n_b\right).$$
 (77)

This implies, following an induction argument, that $P\left(\frac{\sigma}{\sqrt{2^{n_b}}},0\right) \approx P_{tg}$, which in turn implies that $\frac{\sigma}{\sqrt{2^{n_b}}} \approx C(P_{tg})$, where $C(P_{tg})$ is a function that depends on the target success probability. We can write:

$$\tilde{\sigma}(dB) \approx 10 \log_{10}(2) \times n_b + 20 \log_{10}[C(P_{tq})] \approx 3.01 dB \times n_b + C'(P_{tq}),$$
(78)

which agrees with the plots presented in Fig. 4.

In particular, the squeezing necessary for the maximum success probability can be estimated analytically. The required condition is that erf $\left(\frac{\sigma}{2}\sqrt{\frac{\pi}{2^n}}\right) \approx 1$ (see Eq. (65)), which implies $\sigma \geq 2c\sqrt{\frac{2^n}{\pi}}$ and $s_c = 0$ (see Eq. (38)). Employing Eqs. (65) and (76), we conclude

$$P(\sigma, n-1) \approx 0.5 + 0.5^n$$
, when $\tilde{\sigma}(dB) \ge 10 \log_{10}(2) \times n + 20 \log_{10}\left(\frac{2c}{\sqrt{\pi}}\right) \approx 3.01 dB \times n + C.$ (79)

Here, C is a term which depends on the threshold fidelity, but is independent of n. For example, for c = 2.2 which yields a fidelity F > 0.99, we obtain C = 7.9dB.

For high-fidelity thresholds, the analytical results presented so far are in agreement with numerical simulations. This is illustrated in Fig. 5 which plots the success probability versus squeezing $\tilde{\sigma}(dB)$ for a protocol producing $n_b = 3$ Bell pairs with a fidelity exceeding 0.99, for different values of s_c . The success probability is obtained numerically by

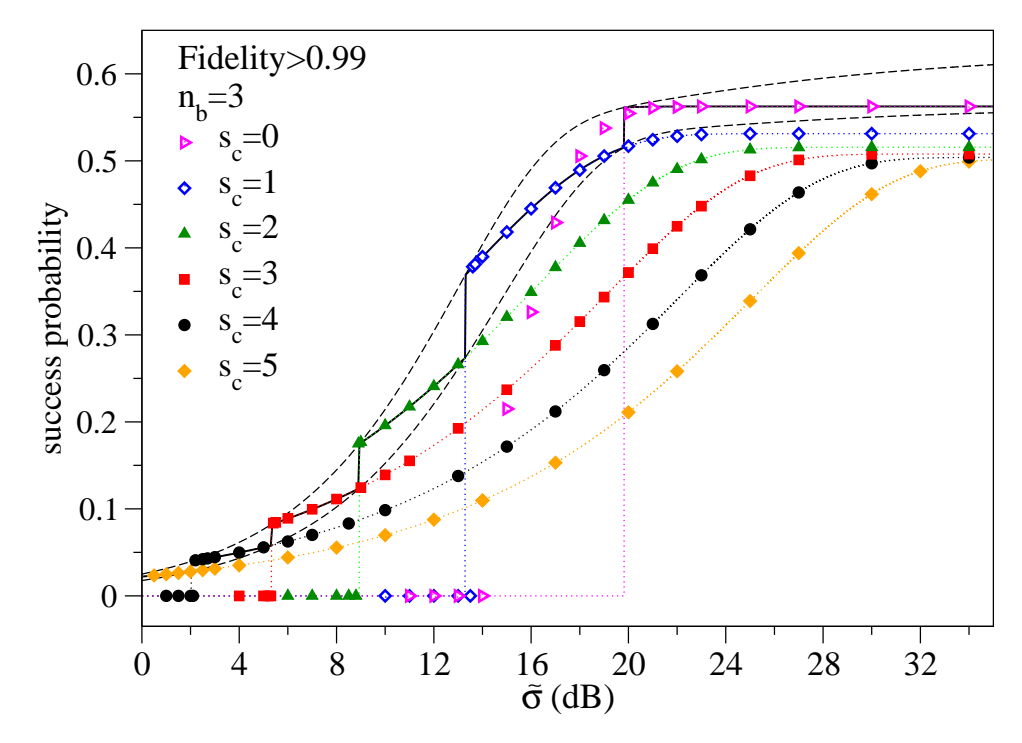


FIG. 5: The protocol success probability versus squeezing $\tilde{\sigma}(dB)$. The symbols are obtained by simulating the protocol steps outlined in Section III for a protocol producing $n_b=3$ Bell states with fidelity F>0.99, for different values of s_c . Since the truncation approximation (Eq. (37)) fails when $\sigma<\sigma_c$ (see Eqs. (39) and (71)), the probability of obtaining high-fidelity Bell states rapidly drops to zero when $\sigma<\sigma_c$, while keeping s_c fixed. The dotted lines correspond to $P(\sigma,s_c,n_b)$ given by Eq. (69) for $\sigma\geq\sigma_c$ and to zero for $\sigma<\sigma_c$. The dashed lines represent $P_{upper}(\sigma,n_b)$ and $P_{lower}(\sigma,n_b)$ given by Eqs. (74) and (75), and the solid line represents the expression for the success probability given by Eq. (72). When $\sigma\approx\sigma_c$, the maximum success probability jumps up because it corresponds to the success probability obtained when s_c is reduced by 1. All analytical results are calculated with c=2.17, a value that best fits the numerical results for a threshold fidelity of 0.99.

simulating the protocol steps outlined at the beginning of Section III and counting all the final states that pass the purification rules summarized at the end of Section III A 1 and have a fidelity exceeding the threshold fidelity. The analytical approximation of the success probability, $P(\sigma, n_b)$, given by Eq. (72), is shown with a continuous line, while $P_{upper}(\sigma, n_b)$ and $P_{lower}(\sigma, n_b)$, described by Eqs. (74) and (75), are shown with dashed lines. Notice the discontinuity of $P(\sigma, n_b)$, which jumps from $P_{lower}(\sigma, n_b)$ to $P_{upper}(\sigma, n_b)$ for values of σ that satisfy Eq. (71), a direct consequence of the discontinuity of $s_c(\sigma, n_b)$ as a function of σ (see Eq. (70)). At these points, σ is large enough that a decrease in s_c by 1, while maintaining the high-fidelity approximation (Eq. (37)), is possible. The decrease in s_c results in a jump in the success probability. On the intervals between the discontinuity points, $P(\sigma, n_b)$ is described by Eq. (69). The best fit between analytical predictions and numerical calculations with F=0.99 fidelity threshold is obtained by taking the cutoff parameter c=2.17 in Eqs. (68), (72), (74) and (75). The good agreement validates the analytical approach and indicates that for a cutoff parameter $c \gtrsim 2.17$, the truncation errors introduced by Eq. (37) are small enough to yield fidelity errors of $\approx 1\%$.

When the value of s_c is not large enough to make the truncation errors in Eq. (37) negligible, the fidelity of the protocol is reduced. Numerical calculations of the success probability versus the threshold fidelity are illustrated in Fig. 6 for different values of s_c for a protocol generating $n_b=4$ Bell pairs. The success probability reaches its maximum when all states passing the purification rules are counted. We identify three regimes for qualitative distinction. In the low squeezing and small s_c regime (for example $s_c=0$ and $s_c=1$ at $\tilde{\sigma}=10dB$ in Fig. 6-a), the fidelity of all the states is low, and the protocol is essentially failing. In the intermediate s_c and squeezing regime, the success probability is small for a protocol with high fidelity threshold (for example, F>0.9), since many states passing the purification rules have low fidelity. Decreasing the threshold fidelity significantly increases the success probability in this case (for example, observe $s_c=2$ at $\tilde{\sigma}=10$ dB in Fig. 6-a and $s_c=0$ and $s_c=1$ at $\tilde{\sigma}=15$ dB in Fig. 6-b). Finally, we have the high-fidelity regime, achieved with large s_c and/or squeezing (see $s_c=3$ at $\tilde{\sigma}=10$ dB in Fig. 6-b). In this regime, all states passing the purification rules have high fidelity

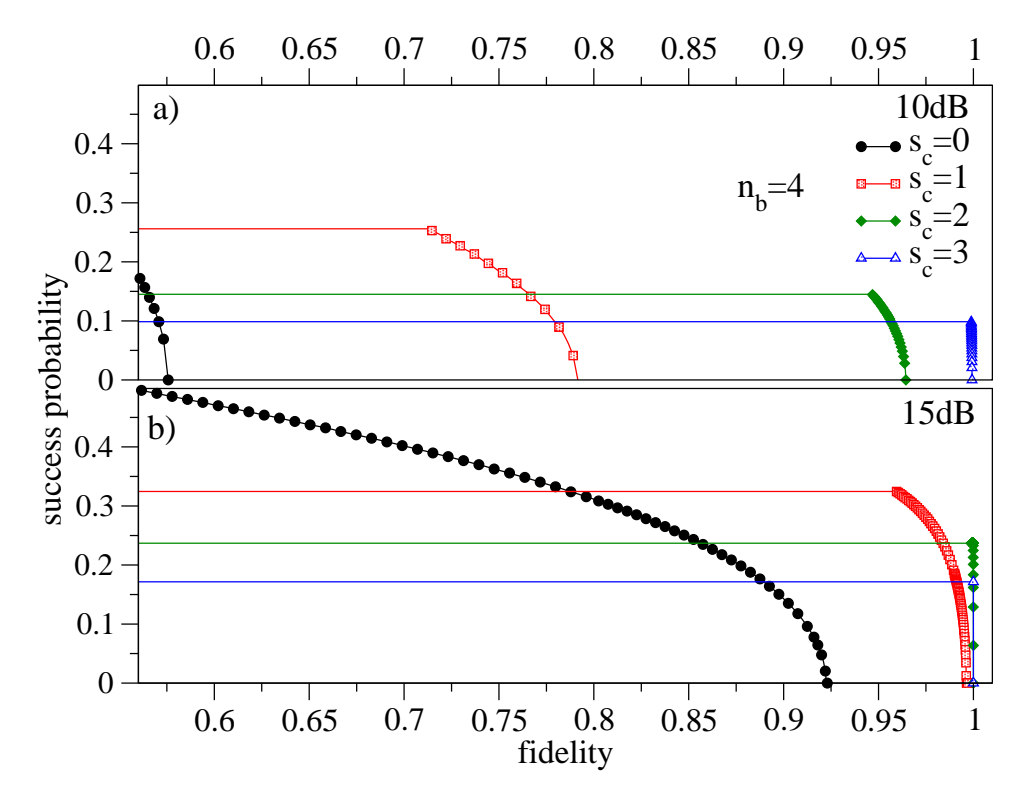


FIG. 6: Success probability versus threshold fidelity for a protocol producing $n_b = 4$ Bell pairs, for a) $\tilde{\sigma} = 10dB$ squeezing and b) $\tilde{\sigma} = 15dB$ squeezing. The success probability increases as the threshold fidelity decreases. When s_c is large enough to satisfy Eq. (39) for a value of $c \gtrsim 2.2$ (green diamond in (b) and blue triangle in (a) and (b)), the success probability is given by Eq. (69) up to a threshold fidelity > 0.99.

(F > 0.99). The success probability is well approximated by Eq. (69).

Although the main advantage of our protocol is the capability to produce multiple Bell pairs, it can also be used to produce single Bell pairs (by taking n=2 and $s_c=0$) with success probabilities reaching 0.75 for squeezing achievable with present technology (i.e., $\tilde{\sigma} \leq 15dB$). This is predicted by Eq. (79) when $\tilde{\sigma} \gtrsim 14dB$ and by numerical calculations shown in Fig. 7, where the success probability versus fidelity is plotted for different values of the squeezing factor. For example, when $\tilde{\sigma} = 10dB$ ($\tilde{\sigma} = 15dB$), our protocol can produce a Bell pair with 0.9 (0.99) fidelity with a success probability of approximately 0.7 (0.75). These success probabilities are significantly larger than the value of 0.5, which represents the upper bound characterizing photonic-qubit protocols with incomplete BSM [6], giving our protocol a potential advantage for generating Bell pairs at a higher rate when employed in optical networks.

IV. Discussions

Several potential impediments to the practical implementation of the protocol in the near future need to be addressed. For example, step 6 of our protocol requires the implementation of the multi-qubit operator D(-t) (see Eq. (12)) at one of the nodes. This necessitates the implementation of two multi-qubit QFTs (see Fig. 3b), which requires $\mathcal{O}(n^2)$ two-qubit gates [26] (such as CNOT gates). For large-sized registers, this can be challenging since the limited fidelity of two-qubit gates with current technology restricts the number of two-qubit gates that can be implemented. However the implementation for small n is feasible with current technology. For example, the QFT for n=2 requires only one CNOT gate.

In our protocol, the number of Bell pairs that can be produced increases with increasing squeezing, as implied by Eq. (79). The current technological limitations in squeezing restrict the protocol's feasibility to generating only a small number of Bell pairs at present. However, significant efforts to advance squeezing technology are underway in many groups [25, 27–29], enhancing the relevance of our protocol for near-future applications.

While we considered squeezed vacuum here, the protocol also works with other choices of the initial CV wavefunction. The essential requirement is that the function $\hat{h}_{x_D}(p)$, defined in Eq. (24), has a narrow support centered around

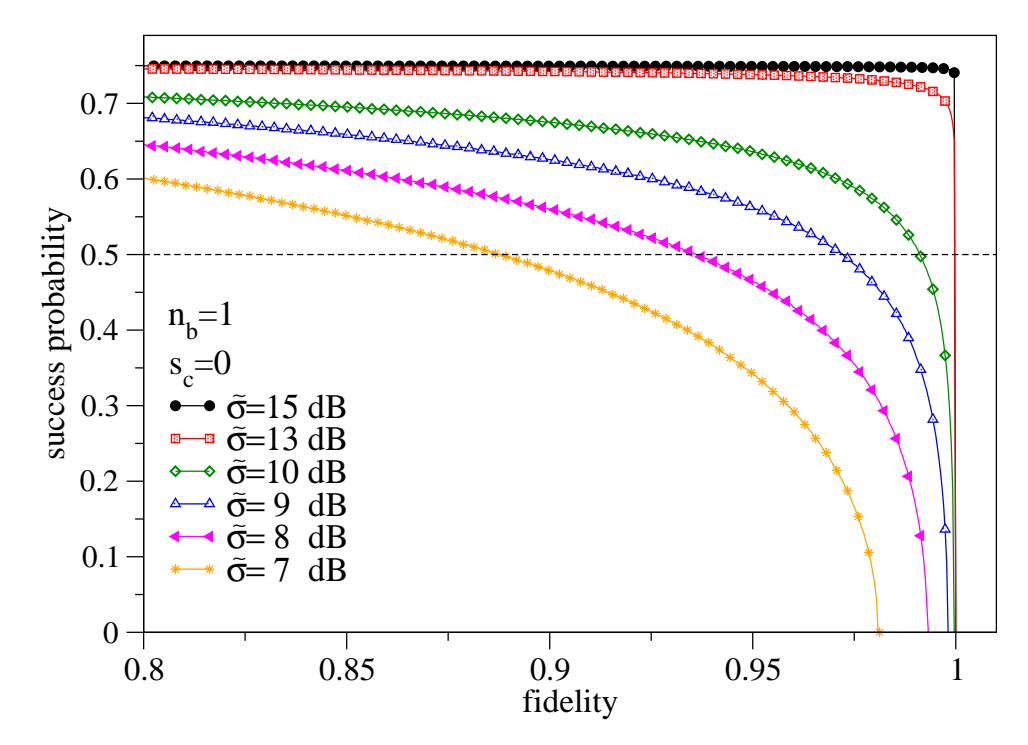


FIG. 7: Success probability versus threshold fidelity for a protocol producing one Bell pair. For a threshold fidelity F > 0.8, the success probability is significantly larger than 0.5 for squeezing values achievable with present-day technology.

p=0 within a good approximation. For instance, we implemented the protocol using a rectangular g(x), although we did not conduct a comprehensive investigation of its efficiency in this context. Exploring alternative choices could prove beneficial for optimizing the protocol's practical implementation under varying technological constraints.

An essential goal of any entanglement generation protocol is to generate high-fidelity Bell pairs at a high rate for quantum networks. For example, a direct application of our protocol would be a quantum repeater designed to distribute Bell pairs between multi-qubit end nodes separated by long distances. Between the end nodes, a series of intermediary nodes will be placed, each containing two registers of n qubits. Midway between these qubit nodes, optical nodes equipped with beam splitters and homodyne detectors are positioned. These optical nodes are connected via fiber optics to the adjacent qubit nodes. The maximum distance between the intermediary nodes is constrained by tolerable loss in fiber optics, which will be estimated in future work. Our protocol constitutes the first step in the long-distance entanglement distribution process, generating n_b Bell pairs between adjacent qubit nodes by employing beam splitters and homodyne measurements at the optical nodes. The next step will involve local and deterministic qubit Bell measurements at the intermediary nodes, progressively extending the range of entanglement. The final outcome will be multiple Bell pairs shared between the end nodes. Various purification protocols may also need to be considered in realistic scenarios to compensate for noise-induced errors.

Since the CV-DV hybrid protocol presented here yields multiple entangled qubits, it is worth evaluating its efficiency against other protocols capable of producing multiple Bell pairs. For example, qubit-based DV-DV protocols can generate at most a single Bell pair per swapping event. To produce multiple Bell pairs, they must be applied multiple times. The efficiency of DV-DV protocols in generating multiple Bell pairs depends on the employed signal transmission scheme (multiplexing), success probability, qubit coherence time, signal loss, and distillation procedures.

Other hybrid CV-DV protocols capable of generating multiple Bell pairs should also be considered for comparison. For instance, the protocol introduced in Ref. [16], which employs a dispersive light-matter interaction between a coherent CV mode and qubits, could be generalized. By controlling the interaction strength or duration, the phase of the coherent mode can be made dependent on the number j that defines the DV state (see Eq. (4)). We envision two possible approaches for the next step. First, two distinct coherent modes could be used: one interacting with the DV register at Alice and the other with the DV register at Bob, after which both modes would be sent to Charlie and passed through a beam splitter. Alternatively, a single CV mode could interact with both DV registers. In both cases, homodyne measurements on the CV states (or the single CV state in the latter case) could, in principle, project, with a finite success probability, a state that has a large overlap with a multi-Bell-pair state. As in the protocol introduced

in Ref. [16], achieving high fidelity will likely require large-amplitude coherent states, with the amplitude increasing as n increases. Beam loss is expected to impose significant constraints on the protocol's success probability.

Many factors influence the Bell pair generation rate, including quantum and classical signal loss in optical fibers, homodyne and qubit measurement errors, distillation protocols, memory decoherence, and signal multiplexing and parallelization schemes. Our protocol, capable of generating both multiple and single Bell pairs with high success probability, holds promise for increasing the Bell pair generation rate. However, a quantitative estimate can only be made after integrating the protocol into an optimized quantum repeater or networking framework while accounting for loss and errors. For example, by introducing fictitious beam splitters coupled to vacuum modes, one can model the effects of beam loss and beam mismatch in fiber-optic setups and homodyne detectors. Phase noise in homodyne detection can be accounted for by introducing quadrature phase shifts. Electronic noise in photodiodes can be represented by adding a small classical error to the measured quadrature values. We plan to investigate these effects on our protocol in future work.

V. Conclusions

We present a hybrid DV-CV entanglement generation protocol using linear optics and homodyne measurements, capable of producing multiple Bell pairs per protocol iteration with ≈ 0.5 probability. Two multi-qubit registers of size n at two separate nodes are locally entangled with squeezed vacuum optical modes. The optical modes are sent to a third party, passed through a 50 : 50 beam-splitter, and undergo homodyne quadrature measurement. The outcome of the homodyne measurement is transmitted back to the multi-qubit nodes through classical channels. Local operations, such as single qubit phase rotations with angles determined by the homodyne measurement outcome and QFT, are then applied to the multi-qubit registers, followed by the measurement of $1 + s_c$ qubits at each node. The success of the protocol depends on the outcomes of the homodyne and qubit measurements. When successful, the protocol produces $n_b = n - 1 - s_c$ qubits with high fidelity.

The efficiency of our protocol is limited by the technological constraints in squeezing optical modes. With sufficiently large squeezing (see Eq. (79)), only one qubit at each register needs to be measured, and the protocol's success probability for producing n-1 Bell pairs with a fidelity exceeding 0.99 reaches $0.5 + 0.5^n$. The success probability and fidelity decreases with decreasing squeezing strength. The fidelity can be increased by measuring more qubits (i.e. by increasing s_c), but this decreases both the success probability and the final number of Bell pairs. To maintain a fixed success probability, an additional squeezing of 3.01dB is required for every extra Bell pair produced.

Our protocol can also be used to produce high-fidelity single Bell pairs with a success probability reaching 0.75 for squeezing strengths achievable with current technology.

Both the capability to generate multiple Bell pairs and the ability to produce a single Bell pair with a high success probability demonstrate the potential of our protocol to advance the development of new quantum repeaters and quantum networks with high-rate Bell pair generation.

Our protocol can generate multiple Bell pairs even with small squeezing, easily achievable with current experimental techniques, albeit with a low success probability that limits its effectiveness. However, this opens up the possibility for experimental testing.

VI. Acknowledgments

This manuscript has been authored by Fermi Research Alliance, LLC under Contract No. DE-AC02-07CH11359 with the U.S. Department of Energy, Office of Science, Office of High Energy Physics. The research team are partially supported by the U.S. Department of Energy, Office of Science Advanced Scientific Computing Research program under FWP FNAL 23-24.

^[1] M. Żukowski, A. Zeilinger, M. A. Horne, and A. K. Ekert, "Event-ready-detectors" Bell experiment via entanglement swapping, Phys. Rev. Lett. 71, 4287 (1993).

^[2] J.-W. Pan, D. Bouwmeester, H. Weinfurter, and A. Zeilinger, Experimental entanglement swapping: Entangling photons that never interacted, Phys. Rev. Lett. 80, 3891 (1998).

^[3] P. van Loock and S. L. Braunstein, Unconditional teleportation of continuous-variable entanglement, Phys. Rev. A 61, 010302 (1999).

^[4] N. Lütkenhaus, J. Calsamiglia, and K.-A. Suominen, Bell measurements for teleportation, Phys. Rev. A 59, 3295 (1999).

^[5] L. Vaidman and N. Yoran, Methods for reliable teleportation, Phys. Rev. A 59, 116 (1999).

- [6] J. Calsamiglia and N. Lütkenhaus, Maximum efficiency of a linear-optical Bell-state analyzer, Applied Physics B 72, 67 (2001).
- [7] P. G. Kwiat and H. Weinfurter, Embedded Bell-state analysis, Phys. Rev. A 58, R2623 (1998).
- [8] Y.-H. Kim, S. P. Kulik, and Y. Shih, Quantum teleportation of a polarization state with a complete Bell state measurement, Phys. Rev. Lett. 86, 1370 (2001).
- [9] S. D. Barrett, P. Kok, K. Nemoto, R. G. Beausoleil, W. J. Munro, and T. P. Spiller, Symmetry analyzer for nondestructive Bell-state detection using weak nonlinearities, Phys. Rev. A 71, 060302 (2005).
- [10] Z. Jian, Y. Ming, L. Yan, and C. Zhuo-Liang, Nearly deterministic teleportation of a photonic qubit with weak cross-Kerr nonlinearities, Chinese Physics Letters 26, 100301 (2009).
- [11] J. Bai, Q. Guo, L.-Y. Cheng, X.-Q. Shao, H.-F. Wang, S. Zhang, and K.-H. Yeon, Implementation of nonlocal Bell-state measurement and quantum information transfer with weak Kerr nonlinearity, Chinese Physics B 20, 120307 (2011).
- [12] J.-M. Wang, M.-z. Zhu, D. Wang, and L. Ye, Nearly deterministic Bell measurement using quantum communication bus, Quantum Information Processing 16, 63 (2017).
- [13] H. A. Zaidi and P. van Loock, Beating the one-half limit of ancilla-free linear optics Bell measurements, Phys. Rev. Lett. 110, 260501 (2013).
- [14] F. Ewert and P. van Loock, 3/4-efficient Bell measurement with passive linear optics and unentangled ancillae, Phys. Rev. Lett. 113, 140403 (2014).
- [15] M. J. Bayerbach, S. E. D'Aurelio, P. van Loock, and S. Barz, Bell-state measurement exceeding 50% success probability with linear optics, Science Advances 9, eadf4080 (2023), https://www.science.org/doi/pdf/10.1126/sciadv.adf4080.
- [16] P. van Loock, T. D. Ladd, K. Sanaka, F. Yamaguchi, K. Nemoto, W. J. Munro, and Y. Yamamoto, Hybrid quantum repeater using bright coherent light, Phys. Rev. Lett. 96, 240501 (2006).
- [17] W. J. Munro, R. Van Meter, S. G. R. Louis, and K. Nemoto, High-bandwidth hybrid quantum repeater, Phys. Rev. Lett. 101, 040502 (2008).
- [18] A. Macridin, A. C. Y. Li, S. Mrenna, and P. Spentzouris, Bosonic field digitization for quantum computers, Phys. Rev. A 105, 052405 (2022).
- [19] A. Macridin, A. C. Y. Li, and P. Spentzouris, Qumode transfer between continuous- and discrete-variable devices, Phys. Rev. A 109, 032419 (2024).
- [20] L. S. Bishop, J. M. Chow, J. Koch, A. A. Houck, M. H. Devoret, E. Thuneberg, S. M. Girvin, and R. J. Schoelkopf, Nonlinear response of the vacuum Rabi resonance, Nature Phys. 5, 105 (2009).
- [21] H. Walther, B. T. H. Varcoe, B.-G. Englert, and T. Becker, Cavity quantum electrodynamics, Reports on Progress in Physics 69, 1325 (2006).
- [22] A. Cottet, M. C. Dartiailh, M. M. Desjardins, T. Cubaynes, L. C. Contamin, M. Delbecq, J. J. Viennot, L. E. Bruhat, B. Douçot, and T. Kontos, Cavity qed with hybrid nanocircuits: from atomic-like physics to condensed matter phenomena, Journal of Physics: Condensed Matter 29, 433002 (2017).
- [23] A. Blais, A. L. Grimsmo, S. M. Girvin, and A. Wallraff, Circuit quantum electrodynamics, Rev. Mod. Phys. 93, 025005 (2021).
- [24] C. Gerry and P. Knight, *Introductory Quantum Optics* (Cambridge University Press, New York, 2004).
- [25] H. Vahlbruch, M. Mehmet, K. Danzmann, and R. Schnabel, Detection of 15 db squeezed states of light and their application for the absolute calibration of photoelectric quantum efficiency, Phys. Rev. Lett. 117, 110801 (2016).
- [26] M. A. Nielsen and I. Chuang, Quantum computation and quantum information: 10th anniversary edition (2010).
- [27] A. Schönbeck, F. Thies, and R. Schnabel, Opt. Lett. 43, 110 (2018).
- [28] M. Hagemann, J. Zander, A. Schönbeck, and R. Schnabel, 10-db squeeze laser tuneable over half a nanometer around 1550 nm, Opt. Express 32, 7954 (2024).
- [29] J. Li, Y.-P. Wang, J.-Q. You, and S.-Y. Zhu, Squeezing microwaves by magnetostriction, National Science Review 10, 247 (2022).

A. CV entanglement swapping

The continuous-variable entanglement swapping protocol was introduced in [3]. Here, we present a modified version similar to our hybrid protocol. In fact, the hybrid protocol, in the limit of large squeezing and large qubit register sizes, converges to the continuous-variable protocol presented here.

1. Alice starts with two independent modes, 1 and 2:

$$|\chi (\text{step1})\rangle_A = \int |x_1\rangle_A dx_1 \otimes \int |x_2\rangle_A dx_2$$
 (A1)

Similarly, Bob starts with the modes 3 and 4:

$$|\chi \text{ (step 1)}\rangle_B = \int |x_3\rangle_B dx_3 \otimes \int |x_4\rangle_B dx_4$$
 (A2)

The wavefunctions of the modes in Eqs. (A1) and (A2) are unnormalized and describe infinitely squeezed vacuum states, as they can be obtained by taking $\sigma \to \infty$ in Eq. (30).

2. Alice applies the operator $e^{-iX_1 \otimes X_2}$:

$$|\chi\left(\text{step2}\right)\rangle_A = \int e^{-ix_1x_2} |x_1, x_2\rangle_A dx_1 dx_2. \tag{A3}$$

Similarly, Bob applies the operator $e^{-iX_3 \otimes X_4}$:

$$|\chi\left(\text{step2}\right)\rangle_{B} = \int e^{-ix_{3}x_{4}} |x_{3}, x_{4}\rangle_{B} dx_{3}dx_{4}. \tag{A4}$$

3. Alice sends mode 2 to Charlie, and Bob sends mode 3 to Charlie. Charlie sends the modes 2 and 3 thorough a 50:50 beam splitter,

$$|\chi \text{ (step 3)}\rangle_{ABC} = \int dx_1 dx_2 dx_3 dx_4 e^{-ix_1 x_2} e^{-ix_3 x_4} |x_1, x_4\rangle_{AB} \left| \frac{x_2 + x_3}{\sqrt{2}}, \frac{-x_2 + x_3}{\sqrt{2}} \right\rangle_C.$$
 (A5)

4. Employing homodyne measurement, Charlie measures the quadrature X for one mode and the quadrature P for the other mode. Denoting the measurement results by x_D and p_D , the state becomes (see Eq. (B1)):

$$|\chi (\text{step4})\rangle_{AB} = \int dx_1 dx_4 |x_1, x_4\rangle_{AB} \frac{1}{\sqrt{2\pi}} \int dx_2 dx_3 e^{-i(x_1 x_2 + x_3 x_4)} \delta \left(x_D - \frac{x_2 + x_3}{\sqrt{2}} \right) e^{-ip_D \frac{-x_2 + x_3}{\sqrt{2}}}$$

$$= \sqrt{2} e^{-ip_D x_D} \int dx |x + \sqrt{2} p_D, x\rangle_{AB} e^{-i\sqrt{2} x_D x}$$
(A6)

5. Bob applies the displacement operator $e^{i\sqrt{2}x_DX_4}$:

$$\left|\chi\left(\text{step5}\right)\right\rangle_{AB} = \sqrt{2}e^{-ip_Dx_D} \int dx \left|x + \sqrt{2}p_D, x\right\rangle_{AB}.$$
 (A7)

6. Alice applies the displacement operator $e^{i\sqrt{2}p_DP_1}$:

$$|\chi \text{ (step 6)}\rangle_{AB} = \sqrt{2}e^{-ip_D x_D} \int dx |x, x\rangle_{AB}.$$
 (A8)

To conclude, by performing homodyne measurements at Charlie, the protocol produces an entangled state between the mode 1 at Alice and mode 4 at Bob.

B. Homodyne measurement

The result of the homodyne measurement is obtained by applying the projector operator $|x_D, p_D\rangle\langle x_D, p_D|$ to the state described by Eq. (22). Considering that

$$\langle x_D, p_D | \frac{x_2 + x_3}{\sqrt{2}}, \frac{-x_2 + x_3}{\sqrt{2}} \rangle = \delta \left(x_D - \frac{x_2 + x_3}{\sqrt{2}} \right) \frac{1}{\sqrt{2\pi}} e^{-ip_D \frac{-x_2 + x_3}{\sqrt{2}}},$$
 (B1)

the post-measurement state becomes:

$$|\chi (\text{step4})\rangle_{AB} = \frac{1}{2^{n} \sqrt{P(x_{D}, p_{D})}} \sum_{j,k=0}^{2^{n}-1} |j,k\rangle_{AB} \frac{1}{\sqrt{\pi}} \int dx_{2} dx_{3} e^{-i(\bar{x}_{j}x_{2}+x_{3}\bar{x}_{k})} g(x_{2}) g(x_{3}) \delta \left(\sqrt{2}x_{D} - x_{2} - x_{3}\right) e^{-ip_{D} \frac{-x_{2}+x_{3}}{\sqrt{2}}}$$

$$= e^{-ip_{D}x_{D}} \frac{1}{2^{n} \sqrt{P(x_{D}, p_{D})}} \sum_{j,k=0}^{2^{n}-1} |j,k\rangle_{AB} e^{-i\sqrt{2}x_{D}\bar{x}_{k}} \frac{1}{\sqrt{\pi}} \int dx_{2} g(x_{2}) g(\sqrt{2}x_{D} - x_{2}) e^{i\left(\sqrt{2}p_{D} - \bar{x}_{j} + \bar{x}_{k}\right)x_{2}}$$

$$= \frac{1}{2^{n} \sqrt{P(x_{D}, p_{D})}} \sum_{j,k=0}^{2^{n}-1} e^{-ix_{D} \frac{\bar{x}_{j} + \bar{x}_{k}}{\sqrt{2}}} |j,k\rangle_{AB} \frac{1}{\sqrt{2\pi}} \int dy g(\frac{x_{D} + y}{\sqrt{2}}) g(\frac{x_{D} - y}{\sqrt{2}}) e^{i\left(p_{D} - \frac{\bar{x}_{j} - \bar{x}_{k}}{\sqrt{2}}\right)y}$$

$$= \frac{1}{2^{n} \sqrt{P(x_{D}, p_{D})}} \sum_{j=1}^{2^{n}-1} e^{-ix_{D} \frac{\bar{x}_{j} + \bar{x}_{k}}{\sqrt{2}}} \hat{h}_{x_{D}} \left(p_{D} - \frac{\bar{x}_{j} - \bar{x}_{k}}{\sqrt{2}}\right) |j,k\rangle_{AB},$$

$$(B2)$$

where $\hat{h}_{x_D}(p)$ is defined by Eq. (24).